

# Journal of Mechanics of Materials and Structures

**TRANSIENT THERMAL STRESSES IN A LAMINATED SPHERICAL SHELL  
OF THERMOELECTRIC MATERIALS**

Yue Liu, KaiFa Wang and Baolin Wang

**Volume 14, No. 3**

**May 2019**





## TRANSIENT THERMAL STRESSES IN A LAMINATED SPHERICAL SHELL OF THERMOELECTRIC MATERIALS

YUE LIU, KAI FA WANG AND BAOLIN WANG

Thermoelectric materials have many potential applications in engineering such as in thermoelectric generators, waste heat recovery industry, thermoelectric cooling devices. They can also be used in thermal protection system of supersonic space shuttles to reduce their surface temperatures. On the other hand, multilayered spherical shell structures are important structure type for thermoelectric material applications. This paper presents a transient analysis model to predict the temperature field and the associated thermal stresses in a laminated thermoelectric spherical shell subjected to a sudden temperature increase on its outer surface. The effects of applied electric current density, thermal conductivity and thickness of laminated shells on the temperature and thermal stress distributions have been obtained and shown graphically. Numerical results show that the maximum tensile hoop stress in the laminated shells can be reduced significantly at a specific applied electric current density. The thermal conductivity ratio of laminated shells has significant impact on the maximum stress level in the shells. When the thermal conductivity ratio of the inner layer to the outer layer increases, the maximum tensile hoop stress increases but the maximum compressive hoop stress decreases.

### 1. Introduction

Thermoelectric materials can achieve energy conversion between electricity and heat and are widely applied to engineering applications [Riffat and Ma 2003]. For example, thermoelectric devices can be used for thermoelectric power generation, refrigeration and thermal protection system [Chowdhury et al. 2009; DiSalvo 1999; Zhang et al. 2016; Han et al. 2014; O'Brien et al. 2008; Li et al. 2005]. They also have potential applications in high-temperature superconductor cables in space solar energy stations. Applications of the thermoelectric conversion technology is calling for high efficiency thermoelectric materials [Huang and Duang 2000; Tian et al. 2015]. Thus thermoelectric materials have attracted attentions in the field of materials science. Zhang et al. [2018b] successfully realized n-type BiCuSeO and Seebeck coefficient of BiCuSeO was improved through introducing extra Bi/Cu to fill the Bi/Cu vacancies. Pothin et al. [2018] finished theoretical and experimental work on the tellurium doping of thermoelectric ZnSb and investigated the influence of tellurium on the phase stabilities. In addition, the requirements of structural strength and reliability of the thermoelectric intelligent devices call for a better understanding of the mechanics properties. Thus stress analysis of thermoelectric materials has attracted more and more attentions. A theoretical model to analyze the thermoelectric conversion efficiency of a cracked material provided by Zhang et al. [2017a]. Later, they also studied the effect of cracking on the thermoelectric properties under combined electrical and temperature loadings [2017b]. Song et al. [2018] analyzed

---

*Keywords:* thermoelectric material, laminated structure, superconductor cable, high temperature, thermal stress, thermal protection system.

the thermoelectric field near an elliptic inhomogeneity in an open circuit by using the complex-variable method. Wang [2015] studied effective material properties of thermoelectric composite materials with elliptical fibers. Liu et al. [2017a] provided a mechanical model of a thermoelectric thin film bonded to an elastic substrate. Applications of the thermoelectric conversion techniques in spacecraft have also attracted more and more attentions. The reason is that when the spacecraft cruise at high velocity, there is a severe heating on their outer surface. However, for safe operation, the temperature on the interior of the spacecraft should not be too high. As a result, there is the large temperature difference between the in-wall and the outer surface of spacecraft. It is the prerequisite of the use of the thermoelectric conversion techniques. In addition, the features of thermoelectric materials and devices make them very attractive for meeting the need of the thermal protection system of spacecraft. For example, the features of them include large operating temperature range, easy to control, reliable operation, layout flexibility, adaptability.

Thermoelectric cylindrical and spherical shells are more and more applied to the thermoelectric devices and many researchers studied them in recent years. Yang et al. [2014] obtained thermoelectric field distributions in both homogeneous shell and core-shell composites and analyzed the effective thermoelectric properties of the core-shell composites. Zhang et al. [2018a] studied the effects of interface layers on the performance of annular thermoelectric generators. Liu et al. [2018] presented a transient model to investigate the dynamic characteristics of laminated thermoelectric cylindrical shells and studied the transient thermal stress fields. In engineering practice, the temperature at the outer surface of thermoelectric spherical shell may be suddenly increased, such as for thermal protection system [Hegde et al. 2012; Lu and Liu 2012]. In order to make the design of thermoelectric devices satisfy the requirements of structural strength, dynamic characteristics of thermoelectric spherical shell should be studied. Suggested by the previous studies [Ching and Chen 2007; Frostig and Thomsen 2007; Qin 2005; Qiu et al. 2018; Wu et al. 2016], the transient thermal stress in the thermoelectric shell structures should be researched. In addition, laminated thermoelectric shells attract more and more attention [Liu et al. 2018; Yang et al. 2014]. The dynamic characteristics of laminated spherical shells of thermoelectric materials should be also studied. To our best knowledge, investigation of transient characteristics of homogeneous thermoelectric spherical shell and laminated thermoelectric spherical shells is very limited.

The aim of current paper is to propose a transient model to study the transient temperature and thermal stress fields in both homogeneous and laminated thermoelectric spherical shells. By using the technique of separation of variables, we obtain the solutions for temperatures at the steady-state and the transient-state. Some numerical calculations are performed to study the transient characteristics of spherical shell. The influences of applied electric current density, thermal conductivity and the thickness of laminated spherical shells on the temperature field and thermal stress field are investigated. This research can provide some guidelines for the design and optimization of thermoelectric shell devices.

## 2. Transient model of the homogeneous thermoelectric spherical shell

Figure 1 shows a homogeneous thermoelectric spherical shell, where  $r$  is the radial coordinate (radius),  $r_1$  is the internal radius and  $r_2$  is the external radius of thermoelectric shell. Note that  $t$  denotes time. Assume that thermoelectric shell is at an initial constant temperature  $T_1$ . For time  $t > 0$ , the temperature of external surface ( $r = r_2$ ) is changed to  $T_2$  and kept at  $T_2$ . For thermoelectric materials, the basic

governing equations in transient state can be expressed as [Wang 2017]

$$\nabla \cdot \mathbf{j} = 0, \quad (1)$$

$$-\nabla \cdot \mathbf{q} - \mathbf{j} \cdot \nabla V = \rho c \frac{\partial T}{\partial t}, \quad (2)$$

$$\mathbf{j} = -\sigma \nabla V - \sigma s \nabla T, \quad (3)$$

$$\mathbf{q} = -\sigma s T \nabla T - (\kappa + \sigma s^2 T) \nabla T, \quad (4)$$

where  $T$  and  $V$  are, respectively, temperature and electric potential;  $\mathbf{j}$  and  $\mathbf{q}$  are, respectively, electric current density and heat flux vector;  $\sigma$ ,  $\kappa$ ,  $s$ ,  $\rho$  and  $c$  are, respectively, electric conductivity, thermal conductivity, Seebeck coefficient, mass density and specific heat. In this work, the symmetric problem is considered so that temperature, electric potential and electric current density depend only on radial coordinate  $r$ . The governing equation for electric current density is rewritten as  $\mathrm{d}j/\mathrm{d}r + 2j/r = 0$ , where  $j$  is the magnitude of current density. As a result,  $j$  can be obtained as  $j = C/r^2$ . A special case is considered and applied electric current density is independent on time, therefore  $C$  is a constant. From (1) to (4), the governing equation for transient temperature can be obtained as

$$\nabla^2 T + \frac{j^2}{\kappa \sigma} = \frac{\rho c}{\kappa} \frac{\partial T}{\partial t}. \quad (5)$$

For 1-D problem of  $T(r, t)$ , equation (5) can be rewritten as

$$\frac{1}{r} \frac{\partial^2}{\partial r^2} (rT) + \frac{j^2}{\kappa \sigma} = \frac{\rho c}{\kappa} \frac{\partial T}{\partial t}. \quad (6)$$

The solution to (6) can be expressed as  $T(r, t) = T_s(r) + T_h(r, t)$ , where  $T_s(r)$  is the steady part of the solution,  $T_h(r, t)$  is the transient part of the solution. Subscripts  $s$  and  $h$  denote the steady and the transient part, respectively. For 1-D problem of  $T_s(r)$ , the governing equation can be expressed as

$$\frac{1}{r} \frac{\mathrm{d}^2}{\mathrm{d}r^2} (rT_s) + \frac{j^2}{\kappa \sigma} = 0, \quad (7)$$

and boundary conditions are  $T_s(r_1) = T_1$  and  $T_s(r_2) = T_2$ . For 1-D problem of  $T_h(r, t)$ , the governing equation can be expressed as

$$\frac{1}{r} \frac{\partial^2}{\partial r^2} (rT_h) = \frac{\rho c}{\kappa} \frac{\partial T_h}{\partial t}, \quad (8)$$

and corresponding boundary conditions are  $T_h(r_1, t) = 0$  and  $T_h(r_2, t) = 0$ , initial condition is  $T_h(r, 0) = T_1 - T_s(r)$ . New variables  $W_s(r)$  and  $W_h(r, s)$  are introduced by the transform  $W_s(r) = rT_s(r)$  and  $W_h(r, t) = rT_h(r, t)$ . Thus (7) and (8) can be rewritten as

$$\frac{\mathrm{d}^2 W_s}{\mathrm{d}r^2} + \frac{rj^2}{\kappa \sigma} = 0, \quad (9)$$

$$\frac{\partial^2 W_h}{\partial r^2} = \frac{\rho c}{\kappa} \frac{\partial W_h}{\partial t}. \quad (10)$$



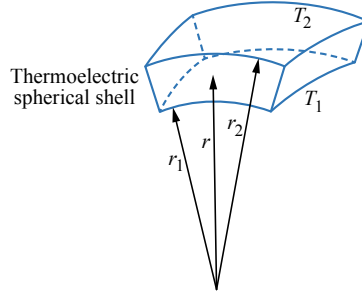


**Figure 1.** The homogeneous thermoelectric spherical shell.

**2.1. The temperature field.** Substituting the expression of  $j$  into (9) gives

$$W_s = -\frac{C^2}{2\kappa\sigma} \frac{1}{r} + C_1 r + C_2, \quad (11)$$

where  $C_1$  and  $C_2$  are unknown constants. From boundary conditions  $C_1$  and  $C_2$  can be solved as

$$C_1 = \frac{r_2 T_2 - r_1 T_1}{r_2 - r_1} - \frac{C^2}{2r_1 r_2 \kappa \sigma}, \quad C_2 = r_1 T_1 + \frac{C^2}{2r_1 \kappa \sigma} - C_1 r_1. \quad (12)$$

The solution to (10) can be expressed as [Hahn and Özişik 2012]

$$W_h(r, t) = \sum_{n=1}^{\infty} \exp\left(-\frac{\kappa}{\rho c} \beta_n^2 t\right) \frac{2}{r_2 - r_1} \sin(\beta_n r) \int_{r_1}^{r_2} \sin(\beta_n r) [r T_1 - W_s(r)] dr, \quad (13)$$

where  $\beta_n = \pi n / (r_2 - r_1)$ ,  $n = 1, 2, 3, \dots$ . Thus  $T(r, t)$  can be obtained as  $T(r, t) = [W_s(r) + W_h(r, t)]/r$ .

**2.2. The thermal stress field.** In this case, only radial strain  $\varepsilon_r$  and hoop strain  $\varepsilon_\theta$  are nonzero. The expressions of them are, respectively,  $\varepsilon_r = du/dr$  and  $\varepsilon_\theta = u/r$ , where  $u$  is radial displacement. The equation of stress equilibrium is  $d\sigma_r/dr + 2(\sigma_r + \sigma_\theta)/r = 0$ . Stress-strain equations are

$$\sigma_r = \frac{E}{(1+\nu)(1-2\nu)} [(1-\nu)\varepsilon_r + 2\nu\varepsilon_\theta - (1+\nu)\alpha\Delta T], \quad (14a)$$

$$\sigma_\theta = \frac{E}{(1+\nu)(1-2\nu)} [\varepsilon_\theta + \nu\varepsilon_r - (1+\nu)\alpha\Delta T], \quad (14b)$$

where  $E$ ,  $\nu$  and  $\alpha$  are Young's modulus, Poisson's ratio and thermal expansion coefficient of the thermoelectric spherical shell, respectively. Note that  $\Delta T$  is temperature increment measured relative to the initial temperature, which can be expressed as  $\Delta T = T(r, t) - T_1$  in this case. Substituting (14a), (14b) and the expressions of  $\varepsilon_r$  and  $\varepsilon_\theta$  into equilibrium equation gives

$$\frac{d}{dr} \left[ \frac{1}{r^2} \frac{d}{dr} (r^2 u) \right] = \frac{1+\nu}{1-\nu} \alpha \frac{d}{dr} (\Delta T). \quad (15)$$

The solution to (15) is

$$u = \frac{1+\nu}{1-\nu} \frac{\alpha}{r^2} \int_{r_1}^r \Delta T r^2 dr + ar + \frac{b}{r^2}. \quad (16)$$

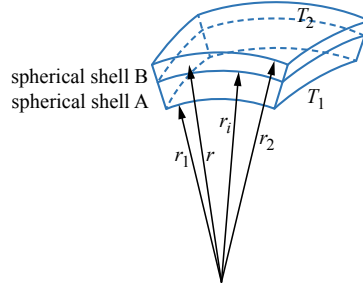


**Figure 2.** The laminated thermoelectric spherical shells.

Thus (14a) and (14b) can be rewritten as

$$\sigma_r = -\frac{2\alpha E}{1-\nu} \frac{1}{r^3} \int_{r_1}^r \Delta T r^2 dr + \frac{Ea}{1-2\nu} - \frac{1}{r^3} \frac{2Eb}{1+\nu}, \quad (17a)$$

$$\sigma_\theta = \frac{\alpha E}{1-\nu} \frac{1}{r^3} \int_{r_1}^r \Delta T r^2 dr + \frac{Ea}{1-2\nu} + \frac{1}{r^3} \frac{Ea}{1+\nu} - \frac{\alpha E \Delta T}{1-\nu}, \quad (17b)$$

where  $a$  and  $b$  are constants. When internal and external surfaces of the shell are stress free,  $a$  and  $b$  can be obtained as

$$a = \frac{2(1-2\nu)b}{r_1^3(1+\nu)}, \quad b = \frac{\alpha(1+\nu)}{1-\nu} \frac{r_1^3}{r_2^3 - r_1^3} \int_{r_1}^{r_2} \Delta T r^2 dr. \quad (18a)$$

When internal surface of shell is fixed and external surface is stress free,  $a$  and  $b$  can be obtained as

$$a = -\frac{b}{r_1^3}, \quad b = -\frac{2\alpha}{1-\nu} \frac{(1-2\nu)(1+\nu)r_1^3}{[r_2^3(1+\nu) + 2(1-2\nu)r_1^3]} \int_{r_1}^{r_2} \Delta T r^2 dr. \quad (18b)$$

When both internal and external surfaces of shell are fixed,  $a$  and  $b$  can be obtained as

$$a = -\frac{b}{r_1^3}, \quad b = -\frac{1+\nu}{1-\nu} \frac{r_1^3 \alpha}{r_1^3 - r_2^3} \int_{r_1}^{r_2} \Delta T r^2 dr. \quad (18c)$$

### 3. The transient model of the laminated thermoelectric spherical shell

As shown in Figure 2, laminated thermoelectric spherical shell is considered which consists of two homogeneous thermoelectric shells, A and B. The interface of the two shells is at  $r_i$ . Note that  $r_1$  and  $r_2$  express, respectively, the internal radius of spherical shell A and the external radius of spherical shell B. Assume that initially the laminated thermoelectric spherical shell is at a constant temperature  $T_1$ . For time  $t > 0$ , temperature of the external surface of shell B ( $r = r_2$ ) is changed to  $T_2$  and kept at  $T_2$ . Similar to the method in Section 2, the temperature field of shell A is  $T_A(r, t) = T_{As}(r) + T_{Ah}(r, t)$  and temperature field of shell B is  $T_B(r, t) = T_{Bs}(r) + T_{Bh}(r, t)$ . The subscripts A and B denote, respectively, the shell A and shell B.

**3.1. The temperature field.** Similar to the method in Section 2, new variables  $W_{As}(r)$ ,  $W_{Bs}(r)$  are introduced by the transform  $W_{As}(r) = rT_{As}(r)$  and  $W_{Bs}(r) = rT_{Bs}(r)$ . These new variables should satisfy (9).

The expressions of them can be obtained as

$$W_{As} = -\frac{C_A^2}{2\kappa_A\sigma_A} \frac{1}{r} + C_{A1}r + C_{A2}, \quad W_{Bs} = -\frac{C_B^2}{2\kappa_B\sigma_B} \frac{1}{r} + C_{B1}r + C_{B2}, \quad (19)$$

where  $C_{A1}$ ,  $C_{A2}$ ,  $C_{B1}$  and  $C_{B2}$  are constants;  $\sigma_A$ ,  $\kappa_A$ ,  $s_A$ , are, respectively, electric conductivity, thermal conductivity and Seebeck coefficient of spherical shell A, and  $\sigma_B$ ,  $\kappa_B$ ,  $s_B$ , are, respectively, electric conductivity, thermal conductivity and Seebeck coefficient of spherical shell B. From boundary conditions we have the equations as

$$r_1 T_1 = -\frac{C^2}{2\kappa_A\sigma_A} \frac{1}{r_1} + C_{A1}r_1 + C_{A2}, \quad r_2 T_2 = -\frac{C^2}{2\kappa_B\sigma_B} \frac{1}{r_2} + C_{B1}r_2 + C_{B2}. \quad (20a)$$

In addition, temperature, electric current density and heat flux are continuous at the interface [Yang et al. 2014], we have the equation as

$$-\frac{C_A^2}{2\kappa_A\sigma_A} \frac{1}{r_i} + C_{A1}r_i + C_{A2} = -\frac{C_B^2}{2\kappa_B\sigma_B} \frac{1}{r_i} + C_{B1}r_i + C_{B2}, \quad (20b)$$

$$C_A = C_B = C, \quad (20c)$$

$$(s_A T_{As} j_A - \kappa_A \nabla T_{As})|_{r=r_i} = (s_B T_{Bs} j_B - \kappa_B \nabla T_{Bs})|_{r=r_i}. \quad (20d)$$

From (20a) to (20d),  $C_{A1}$ ,  $C_{A2}$ ,  $C_{B1}$  and  $C_{B2}$  can be obtained as

$$C_{A1} = -\frac{(\kappa_B r_i^2 \Gamma_1 + \Gamma_3)(r_i - r_2)}{\Gamma_2(r_i - r_2) + (r_i - r_1)\kappa_B r_i^2}, \quad C_{A2} = r_1 T_1 + \frac{C^2}{2r_1\kappa_A\sigma_A} - C_{A1}r_1, \quad (21a)$$

$$C_{B1} = \Gamma_1 + C_{A1} \frac{r_i - r_1}{r_i - r_2}, \quad C_{B2} = r_2 T_2 + \frac{C^2}{2r_2\kappa_B\sigma_B} - C_{B1}r_2, \quad (21b)$$

where

$$\Gamma_1 = \frac{r_1 T_1 - r_2 T_2}{r_i - r_2} + \left( \frac{r_i - r_1}{r_1\kappa_A\sigma_A} + \frac{r_2 - r_i}{r_2\kappa_B\sigma_B} \right) \frac{C^2}{2r_i(r_i - r_2)}, \quad \Gamma_2 = C(s_A - s_B)(r_i - r_1) - [(\kappa_A - \kappa_B)r_1 + \kappa_B r_i]r_i,$$

$$\Gamma_3 = \frac{(\sigma_A - \sigma_B)C^2}{2\sigma_A\sigma_B} + \frac{(r_i - r_1)C^2}{2r_1r_i\kappa_A\sigma_A} [C(s_A - s_B) + r_i(\kappa_A - \kappa_B)] + r_1 T_1 [C(s_A - s_B) + r_i(\kappa_A - \kappa_B)].$$

Similar to Section 2.1,  $T_{Ah}(r, t)$  and  $T_{Bh}(r, t)$  should satisfy (8). The boundary conditions and continuous conditions are

$$T_{Ah}(r_1, t > 0) = 0, \quad (22a)$$

$$T_{Ah}(r_i, t > 0) = T_{Bh}(r_i, t > 0), \quad (22b)$$

$$\kappa_A \frac{\partial T_{Ah}(r, t)}{\partial r} = \kappa_B \frac{\partial T_{Bh}(r, t)}{\partial r}, \quad r = r_i, \quad t > 0, \quad (22c)$$

$$T_{Bh}(r_2, t > 0) = 0. \quad (22d)$$

The initial conditions for  $T_{Ah}(r, t)$  and  $T_{Bh}(r, t)$  are

$$T_{Ah}(r, 0) = T_1 - T_{As}(r), \quad T_{Bh}(r, 0) = T_1 - T_{Bs}(r). \quad (23)$$



$T_{Ah}(r, t)$  and  $T_{Bh}(r, t)$  are [Hahn and Özişik 2012]

$$T_{Ah}(r, t) = \sum_{n=1}^{\infty} \exp(-\beta_n^2 t) \frac{1}{N_n} \varphi_{An}(r) \times \left\{ \rho_A c_A \int_{r_1}^{r_i} r^2 \varphi_{An}(r) [T_1 - T_{As}(r)] dr + \rho_B c_B \int_{r_i}^{r_2} r^2 \varphi_{Bn}(r) [T_1 - T_{Bs}(r)] dr \right\}, \quad (24a)$$

$$T_{Bh}(r, t) = \sum_{n=1}^{\infty} \exp(-\beta_n^2 t) \frac{1}{N_n} \varphi_{Bn}(r) \times \left\{ \rho_A c_A \int_{r_1}^{r_i} r^2 \varphi_{An}(r) [T_1 - T_{As}(r)] dr + \rho_B c_B \int_{r_i}^{r_2} r^2 \varphi_{Bn}(r) [T_1 - T_{Bs}(r)] dr \right\}, \quad (24b)$$

where  $\rho_A, c_A$  are, respectively, mass density and specific heat of spherical shell A,  $\rho_B, c_B$  are, respectively, mass density and specific heat of spherical shell B, and

$$N_n = \rho_A c_A \int_{r_1}^{r_i} r^2 \varphi_{An}^2(r) dr + \rho_B c_B \int_{r_i}^{r_2} r^2 \varphi_{Bn}^2(r) dr, \\ \varphi_{An} = A_{1n} \frac{1}{r} \sin\left(\frac{\beta_n}{\sqrt{\omega_A}} r\right) + B_{1n} \frac{1}{r} \cos\left(\frac{\beta_n}{\sqrt{\omega_A}} r\right), \quad \varphi_{Bn} = A_{2n} \frac{1}{r} \sin\left(\frac{\beta_n}{\sqrt{\omega_B}} r\right) + B_{2n} \frac{1}{r} \cos\left(\frac{\beta_n}{\sqrt{\omega_B}} r\right),$$

where  $A_{1n}, B_{1n}, A_{2n}, B_{2n}, \beta_n$  are the unknown constants and  $\omega_A = \kappa_A / (\rho_A c_A)$ ,  $\omega_B = \kappa_B / (\rho_B c_B)$ .  $A_{1n}, B_{1n}, A_{2n}, B_{2n}$  and  $\beta_n$  are listed in Appendix A. Thus  $T_A(r, t)$  and  $T_B(r, t)$  can be obtained as  $T_A(r, t) = W_{As}(r)/r + T_{Ah}(r, t)$  and  $T_B(r, t) = W_{Bs}(r)/r + T_{Bh}(r, t)$ .

**3.2. The thermal stress field.** Similar to the method in Section 2.2, displacement and stresses in thermoelectric spherical shell A and B can be obtained as

$$u_A = \frac{1 + \nu_A}{1 - \nu_A} \frac{\alpha_A}{r^2} \int_{r_1}^r \Delta T_A r^2 dr + a_{11} r + \frac{b_{12}}{r^2}, \quad (25a)$$

$$\sigma_{Ar} = -\frac{2\alpha_A E_A}{1 - \nu_A} \frac{1}{r^3} \int_{r_1}^r \Delta T_A r^2 dr + \frac{E_A a_{11}}{1 - 2\nu_A} - \frac{1}{r^3} \frac{2E_A b_{12}}{1 + \nu_A}, \quad (25b)$$

$$\sigma_{A\theta} = \frac{\alpha_A E_A}{1 - \nu_A} \frac{1}{r^3} \int_{r_1}^r \Delta T_A r^2 dr + \frac{E_A a_{11}}{1 - 2\nu_A} + \frac{1}{r^3} \frac{E_A b_{12}}{1 + \nu_A} - \frac{\alpha_A E_A \Delta T_A}{1 - \nu_A}, \quad (25c)$$

$$u_B = \frac{1 + \nu_B}{1 - \nu_B} \frac{\alpha_B}{r^2} \int_{r_i}^r \Delta T_B r^2 dr + a_{21} r + \frac{b_{22}}{r^2}, \quad (26a)$$

$$\sigma_{Br} = -\frac{2\alpha_B E_B}{1 - \nu_B} \frac{1}{r^3} \int_{r_i}^r \Delta T_B r^2 dr + \frac{E_B a_{21}}{1 - 2\nu_B} - \frac{1}{r^3} \frac{2E_B b_{22}}{1 + \nu_B}, \quad (26b)$$

$$\sigma_{B\theta} = \frac{\alpha_B E_B}{1 - \nu_B} \frac{1}{r^3} \int_{r_i}^r \Delta T_B r^2 dr + \frac{E_B a_{21}}{1 - 2\nu_B} + \frac{1}{r^3} \frac{E_B b_{22}}{1 + \nu_B} - \frac{\alpha_B E_B \Delta T_B}{1 - \nu_B}, \quad (26c)$$

where  $a_{11}, b_{12}, a_{21}$  and  $b_{22}$  are unknown constants;  $E_A, \nu_A$  and  $\alpha_A$  are, respectively, Young's modulus, Poisson's ratio and thermal expansion coefficient of spherical shell A, and  $E_B, \nu_B$  and  $\alpha_B$  are, respectively, Young's modulus, Poisson's ratio and thermal expansion coefficient of spherical shell B. Assumed that

	$s$ (VK <sup>-1</sup> ) $\times 10^{-6}$	$\sigma$ (Sm <sup>-1</sup> ) $\times 10^3$	$\kappa$ (Wm <sup>-1</sup> K <sup>-1</sup> )	$\rho$ (kgm <sup>-3</sup> )	$c$ (Jkg <sup>-1</sup> K <sup>-1</sup> )	$\alpha$ (K <sup>-1</sup> ) $\times 10^{-5}$	$E$ (GPa)	$\nu$
Shell A	200	110	1.6	7740	154.4	1.68	47	0.3
Shell B	233	47.2	1.22	6760	190	0.42	160	0.4

**Table 1.** Thermoelectric properties of thermoelectric spherical shells A and B [Antonova and Looman 2005; Clin et al. 2009; Gao et al. 2011; Jin 2013; Yang et al. 2014].

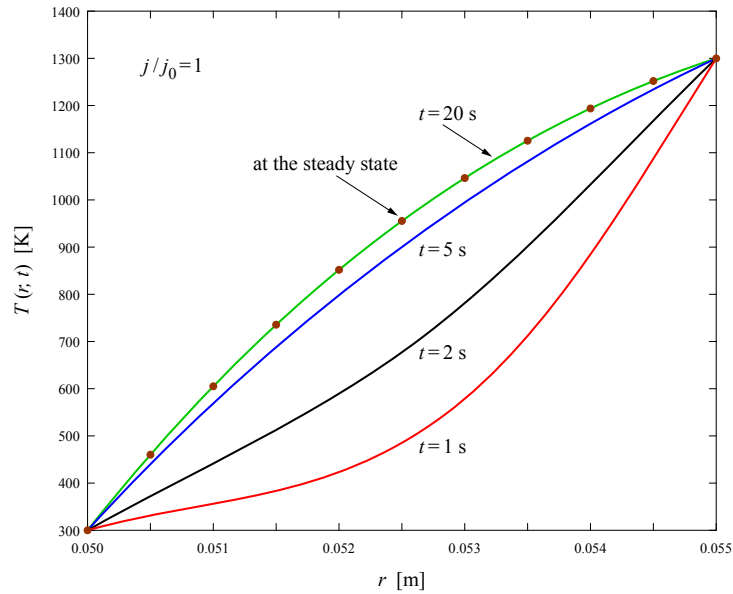
radial displacement and radial stress of spherical shell A and B are continuous at the interface. It means  $u_A(r_i) = u_B(r_i)$  and  $\sigma_{Ar}(r_i) = \sigma_{Br}(r_i)$ .  $a_{11}$ ,  $b_{12}$ ,  $a_{21}$  and  $b_{22}$  are listed in Appendix B.

#### 4. Numerical examples and discussions

The internal and external radii of thermoelectric spherical shell are, respectively, assumed as  $r_1 = 0.05$  m and  $r_2 = 0.055$  m, as shown in Figure 1. For laminated spherical shells, the internal and external radii are, respectively, assumed as  $r_1 = 0.05$  m and  $r_2 = 0.055$  m as shown in Figure 2. The material properties of thermoelectric spherical shell A and shell B are listed in Table 1 [Antonova and Looman 2005; Clin et al. 2009; Gao et al. 2011; Jin 2013; Liu et al. 2017b; Yang et al. 2014]. In addition, assume that material properties of homogeneous thermoelectric spherical shell are the same as thermoelectric shell A in Table 1. Assume that temperature applied on internal surface  $T_1$  is equal to 300 K and temperature applied on the external surface  $T_2$  is equal to 1300 K. In addition,  $V_1$  is applied electric potential on internal surface and value of  $V_1$  is assumed to be zero. A typical value of the electric current density  $j_0 = 3 \times 10^6$  A m<sup>-2</sup> [Wang 2017] is used as the reference value. Assume that the reference electric current density is applied on internal surface of spherical shell. Thus the value of reference constant  $C_0$  is equal to 7500.

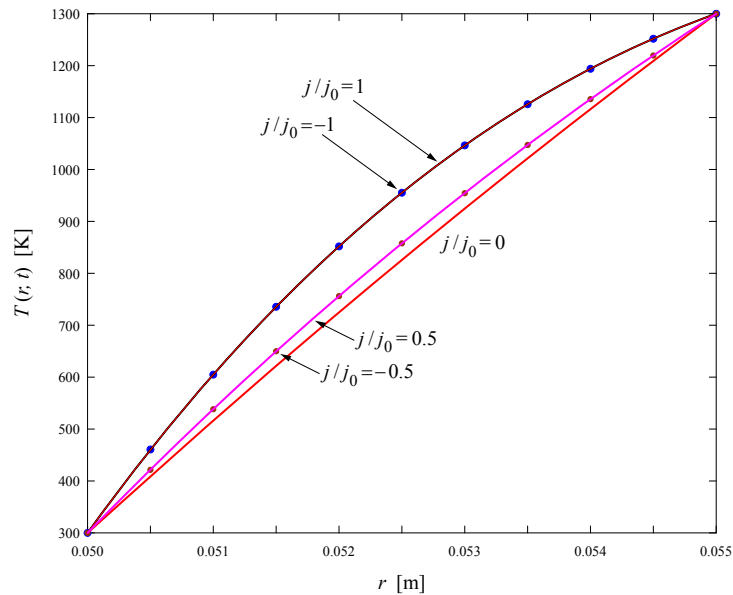
**4.1. The transient temperature field.** Figure 3 shows the temperature profile of homogeneous thermoelectric spherical shell. It is noted that in Figure 3 the normalized current density  $j/j_0$  is assumed to be 1. It shows that temperatures gradually increase with time and become almost steady as time exceeds 20 s in current case. The distribution of temperature is nonlinear, due to Joule heating. Figure 4 shows the influence of applied electric current density on steady-state temperature field of homogeneous thermoelectric spherical shell. Clearly, temperature profiles for positive electric current and negative electric current are almost coincident. This means that direction of applied electric current density does not affect the temperature distribution. The reason is that temperature field of homogeneous thermoelectric spherical shell is affected by the square of applied electric current density  $j$ , which can be found from the equation (11).

Figure 5 shows the temperature profile of laminated thermoelectric spherical shells. The normalized electric current density  $j/j_0$  is assumed to be 1. In this case, temperature increases with time and finally approaches the steady state when time exceeds 20 s. Figure 6 shows the effect of electric current density on steady-state temperature field of laminated thermoelectric spherical shell. Due to thermoelectric effect, heat flux in thermoelectric material is obtained as  $q = sTj - \kappa \nabla T$ , which is affected by electric current density  $j$ . For laminated thermoelectric spherical shells, continuous condition of heat flux is that  $q_A = q_B$



**Figure 3.** Distribution of transient temperature in homogeneous thermoelectric spherical shell for  $j/j_0 = 1$ .

at interface. On the other hand, temperature field is affected by the square of electric current density  $j$  which can be found from governing equation (9). Thus temperature field of laminated spherical shells



**Figure 4.** The influence of applied current density on the temperature field of homogeneous thermoelectric spherical shell under steady state.

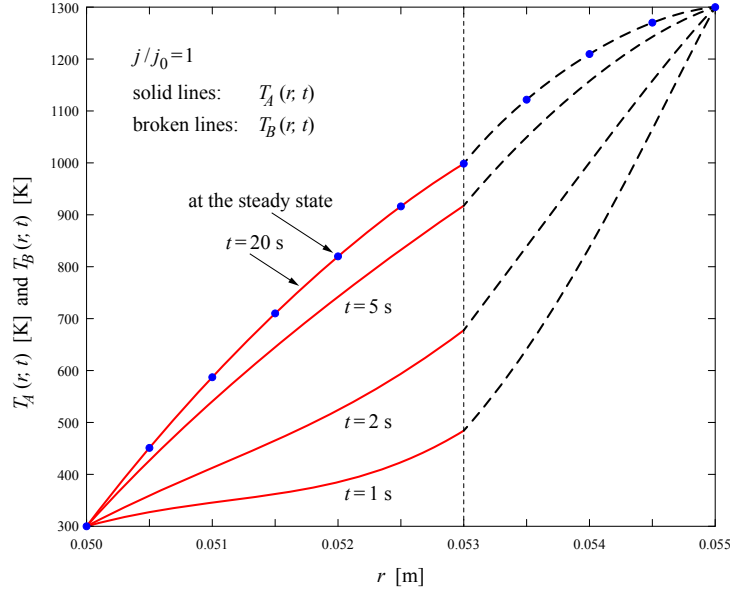


**Figure 5.** Distribution of transient temperature in laminated thermoelectric spherical shell for  $j/j_0 = 1$ .

is dependent on the first and second power of electric current density. Both direction and magnitude of applied current density can affect temperature distribution. If Seebeck coefficient  $s$  is equal to zero (ignore thermoelectric effect), heat flux will be independent of  $j$  and temperature field will be affected only by the second power of electric current density.

**4.2. The transient thermal stress field.** Considering the most common practical situation, the radial stresses at the both internal and external surfaces are assumed to be zero in this subsection. Since the maximum hoop stress is higher than that of radial stress in this case, only distributions of hoop stress are given. As mentioned above, temperature field keep almost steady state as time is greater than 20 s. In addition, the change of temperature field is obvious with time  $t$  varying from 0 s to 10 s and when time  $t$  varying from 10 s to 20 s, the change of temperature field is not obvious. Thus the dynamic variations of hoop stress from 0 s to 10 s are given in this subsection.

Figure 7 shows dynamic hoop stress variations at internal and external surfaces of the homogeneous thermoelectric spherical shell. Since temperature applied on external surface  $T_2$  is higher than initial temperature (hot shock), the region near external surface ( $r_2$ ) is in compressive, whereas a tensile zone is developed at internal surface ( $r_1$ ). Before temperature of spherical shell reaches the steady-state, hoop stress at external surface decreases with time and hoop stress at internal surface increases with time. The transient thermal stress field for positive current density is the same as that for the negative current density. In current case, the maximum compressive stress is at  $r_2$  when time is equal to zero and the maximum tensile stress is at  $r_1$  when the stress field reaches steady state. Figure 8 shows dynamic hoop stress variations at interface, internal and external surfaces of laminated thermoelectric spherical shells. When temperature on external surface ( $r_2$ ) is changed to  $T_2$  ( $T_2 > \text{initial temperature}$ ), the region near external surface of shell B ( $r_2$ ) is in compressive, whereas a tensile zone is developed at interface of shell B ( $r_i$ ).

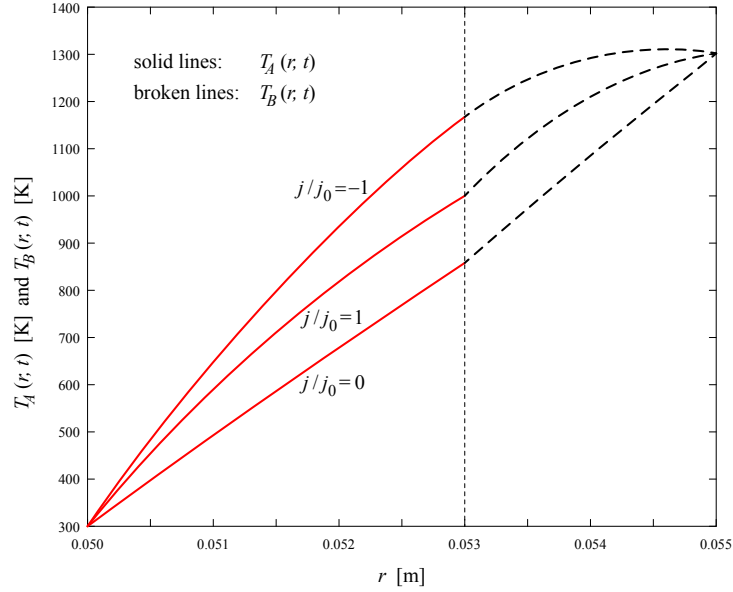


**Figure 6.** The influence of applied current density on the temperature field of laminated thermoelectric spherical shell under steady state.

Due to continuous condition at interface, interface of shell A ( $r_i$ ) is in tensile in a short time after hot shock ( $t < 0.5$  s). When temperature of laminated spherical shells reaches the steady-state, shell A and shell B at interface have the same temperature. In current case, thermal expansion coefficient of shell A is bigger than that of shell B. Thus interface surface of shell A is in compressive at steady-state. Hoop stress at interface  $\sigma_{A\theta}(r_i, t)$  therefore is tensile at the beginning and finally is compressive. Temperature distribution is dependent on both direction and magnitude of applied current density. Thus the transient thermal stress profiles for positive current density is different from that for negative electric current, as shown in Figure 8. In this case, the maximum compressive stress is at external surface of shell B ( $r_2$ ) when time is equal to zero and the maximum tensile stress is at interface of shell B ( $r_i$ ) when the stress field reaches steady state.

**4.3. The influences of thermal conductivity.** Many studies show that reducing the thermal conductivity can improve the thermoelectric figure of merit ( $ZT$ ) but it can also cause thermomechanical issues [Kim et al. 2016]. Thus the influence of thermal conductivity on the thermal stress field should be studied. Figure 9 shows the influence of thermal conductivity on the maximum compressive and tensile hoop stresses. Note that in Figure 9,  $\sigma_{\theta}(r_2, 0)$  and  $s_{\theta s}(r_1)$  are the maximum compressive hoop stress and maximum tensile hoop stress in the shells, respectively. It can be seen that if applied electric current density increases and thermal conductivity decreases, the maximum compressive stress decreases but the maximum tensile stress increases. Influence of thermal conductivity on the maximum tensile stress is more significant than that on the maximum compressive stress. This means that even though lowering thermal conductivity can enhance the thermoelectric figure of merit ( $ZT$ ), it is also likely to cause the structural reliability concerns. Therefore, when we design thermoelectric spherical shell devices, a balance between the thermoelectric performance and structural reliability issue should be made.

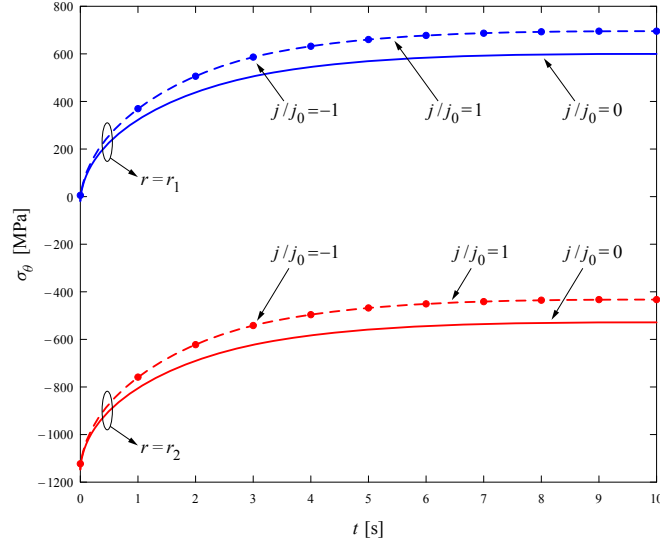


**Figure 7.** The dynamic hoop stress variations at the internal and external surfaces of homogeneous thermoelectric spherical shell (the applied temperature at the internal and external surfaces of shell are, respectively, 300 K and 1300 K).

Figures 10 and 11 show the influence of thermal conductivity on maximum tensile hoop stress and maximum compressive hoop stress of laminated spherical shells, respectively. Note that  $\sigma_{B\theta s}(r_i)$  is the maximum tensile hoop stress of laminated shells in Figure 10 and  $\sigma_{B\theta}(r_2, 0)$  is the maximum compressive

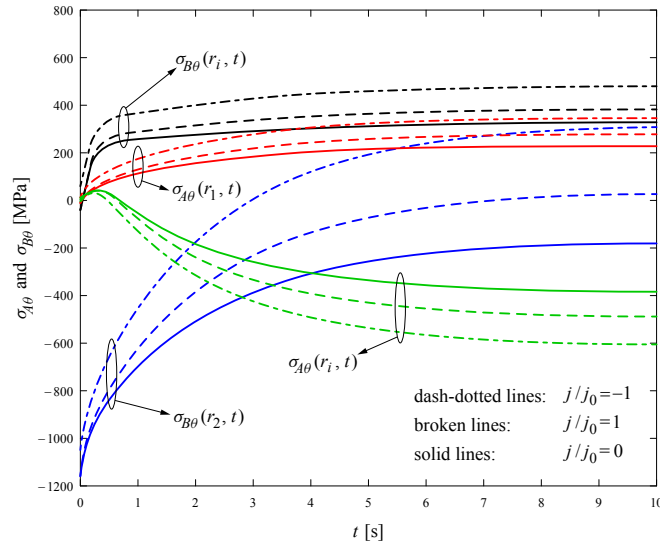


**Figure 8.** The dynamic hoop stress variations at the interface and the internal and external surfaces of laminated thermoelectric spherical shells (the applied temperature at the internal and external surfaces of shell are, respectively, 300 K and 1300 K).



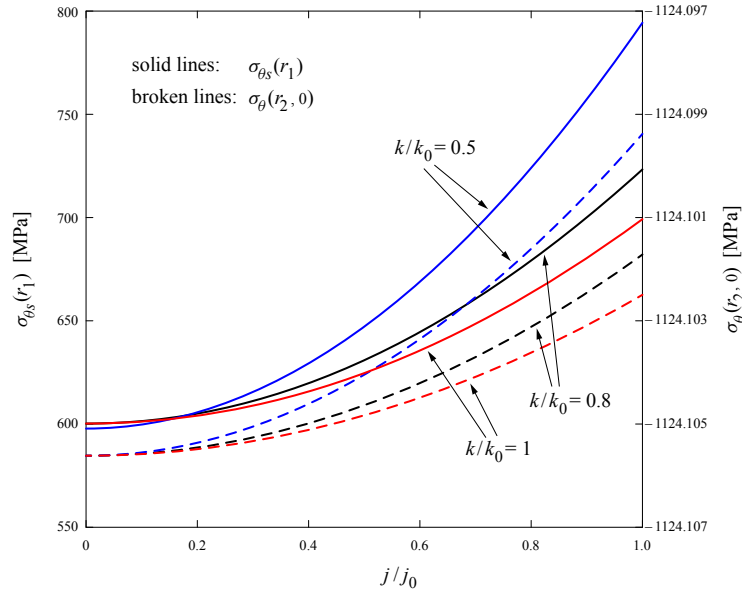


**Figure 9.** The influence of thermal conductivity on the maximum compressive and tensile hoop stresses in homogeneous thermoelectric spherical shell ( $j_0 = C_0/r^2$  where  $C_0 = 7500$ ,  $\kappa_0 = 1.6 \text{ W m}^{-1} \text{ K}^{-1}$ ).

hoop stress of laminated shells in Figure 11. For laminated thermoelectric spherical shells, temperature is a function of the first and second power of electric current density  $j$ . In current case, maximum

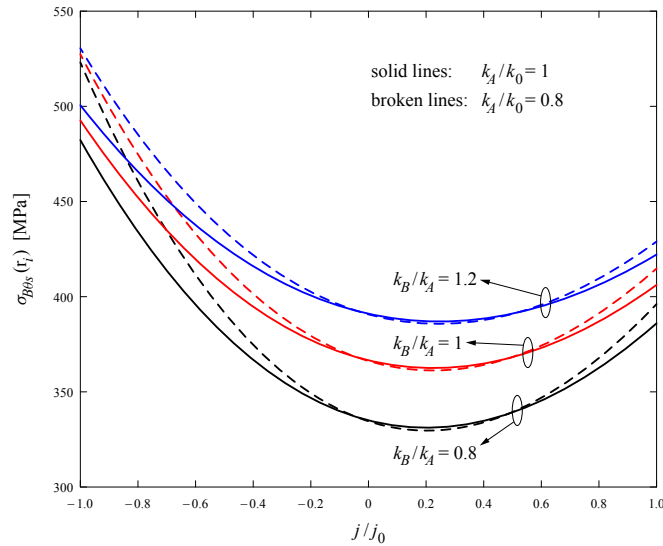


**Figure 10.** The influence of thermal conductivity on the maximum tensile hoop stress in laminated thermoelectric spherical shells ( $j_0 = C_0/r^2$  where  $C_0 = 7500$ ,  $\kappa_0 = 1.6 \text{ W m}^{-1} \text{ K}^{-1}$ ).

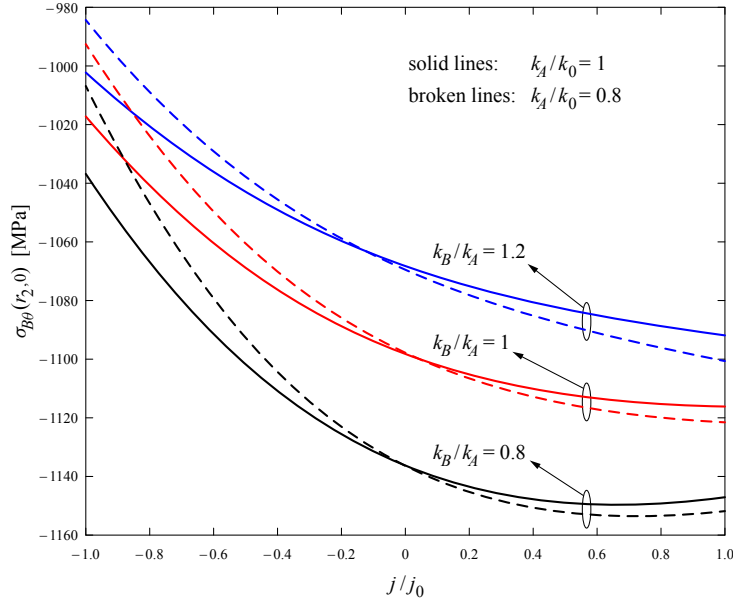


**Figure 11.** The influence of thermal conductivity on the maximum compressive hoop stress in laminated thermoelectric spherical shells ( $j_0 = C_0/r^2$  where  $C_0 = 7500$ ,  $\kappa_0 = 1.6 \text{ W m}^{-1} \text{ K}^{-1}$ ).

tensile hoop stress reaches the lowest value when the value of  $j/j_0$  is around 0.2. When the thermal conductivity ratio of shell A to shell B increases, the maximum tensile hoop stress increases and the maximum compressive hoop stress decreases.

**4.4. The influences of the thickness of laminated shells.** Figures 12 and 13 show, respectively, influence of the thickness of laminated shells on the maximum tensile and compressive hoop stresses. When the laminated thermoelectric spherical shells are used in thermal protection system of supersonic space shuttles, there is the large temperature difference between external surface and internal surface. Thus assumed that  $T_2$  is equal to 1300 K and 1600 K and  $T_1$  is equal to 300 K in this subsection. As mentioned above,  $\sigma_{B\theta s}(r_i)$  and  $\sigma_{B\theta}(r_2, 0)$  are, respectively, the maximum tensile and compressive hoop stresses of laminated shells in Figures 12 and 13. It is noted that increasing  $r_i$  means that the radial thickness of shell B becomes thinner and that of shell A becomes thicker when the radii of internal and external surfaces keep constant. The value of maximum tensile stress is the lowest when the interface is on the middle of laminated shell. It is noted that these lines do not intersect at one point for  $T_2 = 1300 \text{ K}$  or 1600 K, as shown in Figure 13.

## 5. Conclusion

This work constructs a transient mechanical model for laminated thermoelectric spherical shells, considering the coupling of the heat transfer and electric conduction. Notably, a computational code with good human-machine dialogue interface was developed. The code allows us to graphically input data and output the results. The models can evaluate the thermal and mechanical characteristics of materials

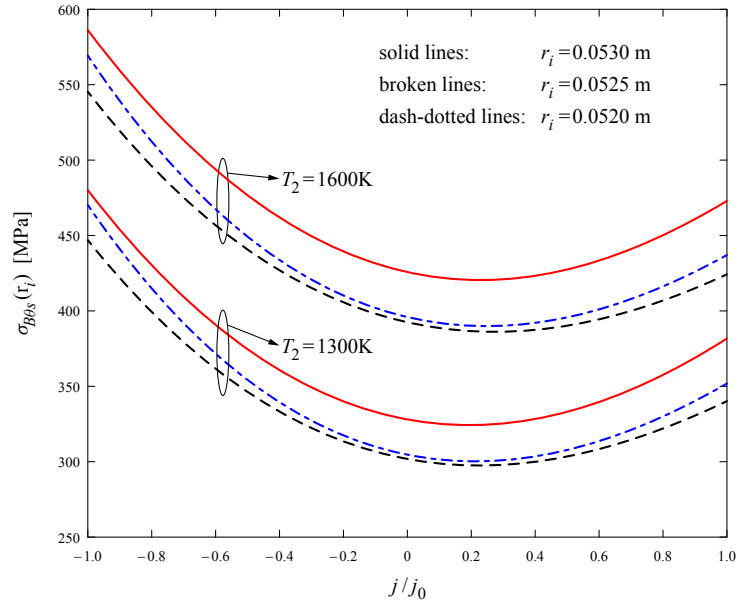


**Figure 12.** The influence of the thickness of laminated shells on the maximum tensile hoop stress in the thermoelectric spherical shell ( $j_0 = C_0/r^2$  where  $C_0 = 7500$ ,  $r_1 = 0.05$  m,  $r_2 = 0.055$  m,  $T_1 = 300$  K).

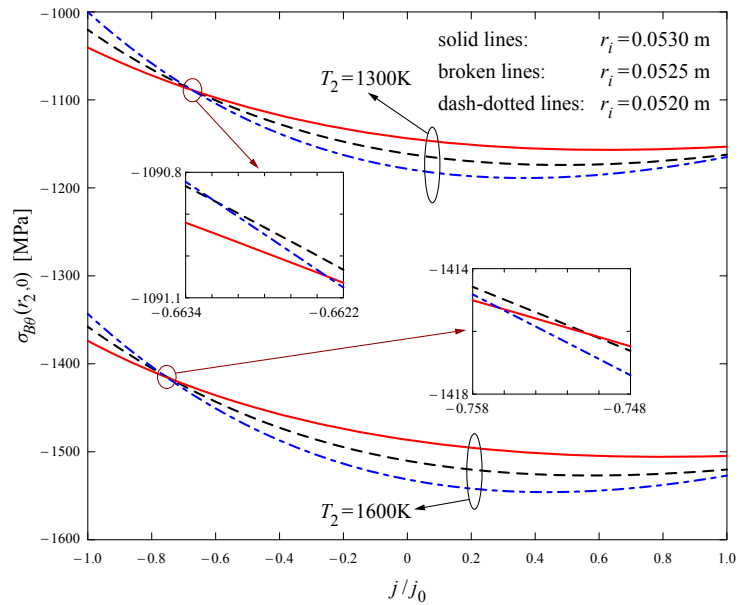


**Figure 13.** The influence of the thickness of laminated shells on the maximum compressive hoop stress in the thermoelectric spherical shell ( $j_0 = C_0/r^2$  where  $C_0 = 7500$ ,  $r_1 = 0.05$  m,  $r_2 = 0.055$  m,  $T_1 = 300$  K).

for temperatures higher than 1300 K, which are very possibly happen thermal protection system of future supersonic space shuttle, and for temperatures as low as 77 K that is possible for high-temperature superconductors in space solar energy station. Numerical results show that specifying the applied electric current density may reduce the maximum tensile stress in the laminated shells. For laminated spherical shells, additional attention for the thermal conductivity ratio of shell A to shell B should be paid. If the thermal conductivity ratio of laminated shells increases, the maximum tensile hoop stress increases but the maximum compressive hoop stress decreases.

### Appendix A

First,  $\varphi_{An}$  and  $\varphi_{Bn}$  should satisfy the following equations [Hahn and Özişik 2012]

$$\varphi_{An}(r_1) = 0, \quad (A1)$$

$$\varphi_{An}(r_i) = \varphi_{Bn}(r_i), \quad (A2)$$

$$\kappa_A \frac{d\varphi_{An}(r)}{dr} = \kappa_B \frac{d\varphi_{Bn}(r)}{dr}, \quad r = r_i, \quad (A3)$$

$$\varphi_{Bn}(r_2) = 0. \quad (A4)$$

Substituting  $\varphi_{An}(r)$  and  $\varphi_{Bn}(r)$  into (A1) to (A4) gives

$$0 = A_{1n} \frac{1}{r_1} \sin\left(\frac{\beta_n}{\sqrt{\omega_A}} r_1\right) + B_{1n} \frac{1}{r_1} \cos\left(\frac{\beta_n}{\sqrt{\omega_A}} r_1\right), \quad (A5)$$

$$A_{1n} \frac{1}{r_i} \sin\left(\frac{\beta_n}{\sqrt{\omega_A}} r_i\right) + B_{1n} \frac{1}{r_i} \cos\left(\frac{\beta_n}{\sqrt{\omega_A}} r_i\right) = A_{2n} \frac{1}{r_i} \sin\left(\frac{\beta_n}{\sqrt{\omega_B}} r_i\right) + B_{2n} \frac{1}{r_i} \cos\left(\frac{\beta_n}{\sqrt{\omega_B}} r_i\right), \quad (A6)$$

$$\begin{aligned} & \frac{\kappa_A}{\kappa_B} A_{1n} \left[ \frac{\beta_n}{\sqrt{\omega_A}} \cos\left(\frac{\beta_n}{\sqrt{\omega_A}} r_i\right) - \frac{1}{r_i} \sin\left(\frac{\beta_n}{\sqrt{\omega_A}} r_i\right) \right] \\ & - \frac{\kappa_A}{\kappa_B} B_{1n} \left[ \frac{1}{r_i} \cos\left(\frac{\beta_n}{\sqrt{\omega_A}} r_i\right) + \frac{\beta_n}{\sqrt{\omega_A}} \sin\left(\frac{\beta_n}{\sqrt{\omega_A}} r_i\right) \right] \\ & = A_{2n} \left[ \frac{\beta_n}{\sqrt{\omega_B}} \cos\left(\frac{\beta_n}{\sqrt{\omega_B}} r_i\right) - \frac{1}{r_i} \sin\left(\frac{\beta_n}{\sqrt{\omega_B}} r_i\right) \right] \\ & - B_{2n} \left[ \frac{1}{r_i} \cos\left(\frac{\beta_n}{\sqrt{\omega_B}} r_i\right) + \frac{\beta_n}{\sqrt{\omega_B}} \sin\left(\frac{\beta_n}{\sqrt{\omega_B}} r_i\right) \right], \quad (A7) \end{aligned}$$

$$0 = A_{2n} \frac{1}{r_2} \sin\left(\frac{\beta_n}{\sqrt{\omega_B}} r_2\right) + B_{2n} \frac{1}{r_2} \cos\left(\frac{\beta_n}{\sqrt{\omega_B}} r_2\right). \quad (A8)$$

Without loss of generality, we choose  $A_{1n} = 1$  [Hahn and Özişik 2012] and  $A_{1n}$ ,  $B_{1n}$ ,  $A_{2n}$  and  $B_{2n}$  can be obtained as

$$A_{1n} = 1, \quad (A9)$$

$$B_{1n} = -\tan\left(\frac{\beta_n}{\sqrt{\omega_A}} r_1\right), \quad (A10)$$

$$A_{2n} = \frac{\cos(\beta_n/\sqrt{\omega_A} r_i) \tan(\beta_n/\sqrt{\omega_A} r_1) - \sin(\beta_n/\sqrt{\omega_A} r_i)}{\cos(\beta_n/\sqrt{\omega_B} r_i) \tan(\beta_n/\sqrt{\omega_B} r_2) - \sin(\beta_n/\sqrt{\omega_B} r_i)}, \quad (\text{A11})$$

$$B_{2n} = -A_{2n} \tan\left(\frac{\beta_n}{\sqrt{\omega_B}} r_2\right). \quad (\text{A12})$$

Equations (A5), (A6), (A7) and (A8) can be expressed in the matrix form. From the requirement that determinant of the coefficients in the matrix should be zero, values of  $\beta_n$  can be obtained.

## Appendix B

Three different boundary conditions are considered: Case 1, both internal and external surfaces of laminated thermoelectric spherical shell are stress free; Case 2, internal surface of shell is fixed, and external surface is stress free; Case 3, both internal and external surfaces of shell are fixed.  $a_{11}$ ,  $b_{12}$ ,  $a_{21}$  and  $b_{22}$  are

$$a_{11} = \Omega_1 b_{12}, \quad (\text{B1})$$

$$b_{12} = \frac{r_i \Omega_3 - \Lambda_5}{\Lambda_1} + \frac{\Lambda_2}{\Lambda_1} b_{22}, \quad (\text{B2})$$

$$a_{21} = \Omega_3 + \Omega_2 b_{22}, \quad (\text{B3})$$

$$b_{22} = \frac{\Lambda_1 \Lambda_6 + \Lambda_3 (r_i \Omega_3 - \Lambda_5) - \Omega_3 \Lambda_1 \Lambda_7}{\Lambda_1 \Lambda_4 - \Lambda_2 \Lambda_3}, \quad (\text{B4})$$

where

$$\begin{aligned} \Lambda_1 &= r_i \Omega_1 + \frac{1}{r_i^2}, \quad \Lambda_2 = r_i \Omega_2 + \frac{1}{r_i^2}, \quad \Lambda_3 = \frac{E_A \Omega_1}{1 - 2\nu_A} - \frac{1}{r_i^3} \frac{2E_A}{1 + \nu_A}, \quad \Lambda_4 = \frac{E_B \Omega_2}{1 - 2\nu_B} - \frac{1}{r_i^3} \frac{2E_B}{1 + \nu_B}, \\ \Lambda_5 &= \frac{1 + \nu_A}{1 - \nu_A} \frac{\alpha_A}{r_i^2} \int_{r_1}^{r_i} \Delta T_A r^2 dr, \quad \Lambda_6 = -\frac{2\alpha_A E_A}{1 - \nu_A} \frac{1}{r_i^3} \int_{r_1}^{r_i} \Delta T_A r^2 dr, \quad \Lambda_7 = \frac{E_B}{1 - 2\nu_B}, \\ \Omega_1 &= \begin{cases} \frac{2(1-2\nu_A)}{r_1^3(1+\nu_A)}, & \text{for case 1,} \\ -\frac{1}{r_1^3}, & \text{for case 2 and case 3,} \end{cases} \quad \Omega_2 = \begin{cases} \frac{2(1-2\nu_B)}{r_2^3(1+\nu_B)}, & \text{for case 1 and case 2,} \\ -\frac{1}{r_2^3}, & \text{for case 3,} \end{cases} \\ \Omega_3 &= \begin{cases} \frac{2\alpha_B(1-2\nu_B)}{1-\nu_B} \frac{1}{r_2^3} \int_{r_i}^{r_2} \Delta T_B r^2 dr, & \text{for case 1 and case 2,} \\ -\frac{1+\nu_B}{1-\nu_B} \frac{\alpha_B}{r_2^3} \int_{r_i}^{r_2} \Delta T_B r^2 dr, & \text{for case 3.} \end{cases} \end{aligned}$$

## Acknowledgment

This research was supported by the Research Innovation Fund of Shenzhen City of China (project nos. JCYJ20170413104256729, JCYJ20170811160538023), the National Natural Science Foundation of China (project nos. 11672084, 11602072, 11972133).

## References

[Antonova and Looman 2005] E. E. Antonova and D. C. Looman, "Finite elements for thermoelectric device analysis in ANSYS", pp. 215–218 in *ICT 2005. 24th International Conference on Thermoelectrics* (Clemson), 2005.

- [Ching and Chen 2007] H. K. Ching and J. K. Chen, “Thermal stress analysis of functionally graded composites with temperature-dependent material properties”, *J. Mech. Mater. Struct.* **2**:4 (2007), 633–653.
- [Chowdhury et al. 2009] I. Chowdhury, K. Prasher, R. Lofgreen, G. Chrysler, S. Narasimhan, R. Mahajan, D. Koester, R. Alley, and R. Venkatasubramanian, “On-chip cooling by superlattice-based thin-film thermoelectrics”, *Nat. Nanotechnol.* **4** (2009), 235–238.
- [Clin et al. 2009] T. Clin, S. Turenne, D. Vasilevskiy, and R. A. Masut, “Numerical simulation of the thermomechanical behavior of extruded bismuth telluride alloy module”, *J. Electron. Mater.* **38**:7 (2009), 994–1001.
- [DiSalvo 1999] F. J. DiSalvo, “Thermoelectric cooling and power generation”, *Science* **285**:5428 (1999), 703–706.
- [Frostig and Thomsen 2007] Y. Frostig and O. T. Thomsen, “Buckling and nonlinear response of sandwich panels with a compliant core and temperature-dependent mechanical properties”, *J. Mech. Mater. Struct.* **2**:7 (2007), 1355–1380.
- [Gao et al. 2011] J.-L. Gao, Q.-G. Du, X.-D. Zhang, and X.-Q. Jiang, “Thermal stress analysis and structure parameter selection for a  $\text{Bi}_2\text{Te}_3$ -based thermoelectric module”, *J. Electron. Mater.* **40**:5 (2011), 884–888.
- [Hahn and Özişik 2012] D. W. Hahn and M. N. Özişik, *Heat conduction*, 3rd ed., John, 2012.
- [Han et al. 2014] X.-Y. Han, J. Wang, and H.-F. Cheng, “Investigation of thermoelectric SiC ceramics for energy harvesting applications on supersonic vehicles leading-edges”, *Bull. Mater. Sci.* **37**:1 (2014), 127–132.
- [Hegde et al. 2012] G. M. Hegde, V. Kulkarni, M. Nagaboopathy, and K. P. J. Reddy, “Structure and morphology studies of chromium film at elevated temperature in hypersonic environment”, *Bull. Mater. Sci.* **35**:3 (2012), 341–345.
- [Huang and Duang 2000] B. J. Huang and C. L. Duang, “System dynamic model and temperature control of a thermoelectric cooler”, *Int. J. Refriger.* **23**:3 (2000), 197–207.
- [Jin 2013] Z.-H. Jin, “Buckling of thin film thermoelectrics”, *Int. J. Fract.* **180**:1 (2013), 129–136.
- [Kim et al. 2016] H. S. Kim, T. Wang, W. Liu, and Z. Ren, “Engineering thermal conductivity for balancing between reliability and performance of bulk thermoelectric generators”, *Adv. Funct. Mater.* **26**:21 (2016), 3678–3686.
- [Li et al. 2005] Y.-Z. Li, C. Wei, L. Yuan, and J. Wang, “Simulation of micro spacecraft active temperature control system using thermoelectric cooler”, *Chinese J. Mech. Eng.* **41** (2005), 149–152. in Chinese.
- [Liu et al. 2017a] Y. Liu, B. L. Wang, and C. Zhang, “Mechanical model for a thermoelectric thin film bonded to an elastic infinite substrate”, *Mech. Mater.* **114** (2017), 88–96.
- [Liu et al. 2017b] Y. Liu, B. L. Wang, and C. Zhang, “Thermoelastic behavior of a thermoelectric thin-film attached to an infinite elastic substrate”, *Philos. Mag.* **97**:1 (2017), 43–57.
- [Liu et al. 2018] Y. Liu, K. F. Wang, and B. L. Wang, “Mechanics modeling of dynamic characteristics of laminated thermoelectric cylindrical shells”, *Appl. Thermal Eng.* **136** (2018), 730–739.
- [Lu and Liu 2012] H.-B. Lu and W.-Q. Liu, “Numerical investigation on properties of attack angle for an opposing jet thermal protection system”, *Chinese Phys. B* **21**:8 (2012), 084401.
- [O’Brien et al. 2008] R. C. O’Brien, R. M. Ambrosi, N. P. Bannister, S. D. Howe, and H. V. Atkinson, “Safe radioisotope thermoelectric generators and heat sources for space applications”, *J. Nucl. Mater.* **377**:3 (2008), 506–521.
- [Pothin et al. 2018] R. Pothin, R. M. Ayril, A. Berche, P. Ziolkowski, G. Oppitz, and P. Jund, “Computational and experimental analysis on Te-doped ZnSb thermoelectric material”, *Mater. Res. Bull.* **101** (2018), 90–99.
- [Qin 2005] Q.-H. Qin, “2D Green’s functions of defective magneto-electroelastic solids under thermal loading”, *Eng. Anal. Bound. Elem.* **29**:6 (2005), 577–585.
- [Qiu et al. 2018] Y. Qiu, H. Wu, J. Wang, J. Lou, Z. Zhang, A. Liu, and G. Chai, “The enhanced piezoelectricity in compositionally graded ferroelectric thin films under electric field: a role of flexoelectric effect”, *J. Appl. Phys.* **123**:8 (2018), 084103.
- [Riffat and Ma 2003] S. B. Riffat and X. Ma, “Thermoelectrics: a review of present and potential applications”, *Appl. Thermal Eng.* **23**:8 (2003), 913–935.
- [Song et al. 2018] K. Song, H. P. Song, and C. F. Gao, “Unavoidable electric current caused by inhomogeneities and its influence on measured material parameters of thermoelectric materials”, *J. Appl. Phys.* **123**:12 (2018), 124105.
- [Tian et al. 2015] H. Tian, X. Sun, Q. Jia, X. Liang, G. Shu, and X. Wang, “Comparison and parameter optimization of a segmented thermoelectric generator by using the high temperature exhaust of a diesel engine”, *Energy* **84** (2015), 121–130.



- [Wang 2015] Y.-Z. Wang, “Effective material properties of thermoelectric composites with elliptical fibers”, *Appl. Phys. A Mater. Sci. Process.* **119**:3 (2015), 1081–1085.
- [Wang 2017] B. L. Wang, “A finite element computational scheme for transient and nonlinear coupling thermoelectric fields and the associated thermal stresses in thermoelectric materials”, *Appl. Thermal Eng.* **110** (2017), 136–143.
- [Wu et al. 2016] H. Wu, L. Li, G. Chai, F. Song, and T. Kitamura, “Three-dimensional thermal weight function method for the interface crack problems in bimaterial structures under a transient thermal loading”, *J. Therm. Stresses* **39**:4 (2016), 371–385.
- [Yang et al. 2014] Y. Yang, C. Gao, and J. Li, “The effective thermoelectric properties of core-shell composites”, *Acta Mech.* **225**:4-5 (2014), 1211–1222.
- [Zhang et al. 2016] G. Zhang, K. Jiao, Z. Niu, H. Diao, Q. Du, H. Tian, and G. Shu, “Power and efficiency factors for comprehensive evaluation of thermoelectric generator materials”, *Int. J. Heat Mass Transf.* **93** (2016), 1034–1037.
- [Zhang et al. 2017a] A. B. Zhang, B. L. Wang, J. Wang, J. K. Du, C. Xie, and Y. A. Jin, “Thermodynamics analysis of thermoelectric materials: influence of cracking on efficiency of thermoelectric conversion”, *Appl. Thermal Eng.* **127** (2017), 1442–1450.
- [Zhang et al. 2017b] A. B. Zhang, B. L. Wang, J. Wang, J. K. Du, and C. Xie, “Effect of cracking on the thermoelectric conversion efficiency of thermoelectric materials”, *J. Appl. Phys.* **121**:4 (2017), 045105.
- [Zhang et al. 2018a] A. B. Zhang, B. L. Wang, D. D. Pang, L. W. He, J. Lou, J. Wang, and J. K. Du, “Effects of interface layers on the performance of annular thermoelectric generators”, *Energy* **147** (2018), 612–620.
- [Zhang et al. 2018b] X. Zhang, D. Feng, J. He, and L.-D. Zhao, “Attempting to realize n-type BiCuSeO”, *J. Solid State Chem.* **258** (2018), 510–516.

Received 21 Nov 2018. Revised 8 Apr 2019. Accepted 1 Jun 2019.

YUE LIU: 750310541@qq.com

Harbin Institute of Technology, Shenzhen, 518055, China

KAI FA WANG: wangkf@hit.edu.cn

Harbin Institute of Technology, Shenzhen, 518055, China

BAOLIN WANG: wangbl@hit.edu.cn

Harbin Institute of Technology, Shenzhen, 518055, China



# JOURNAL OF MECHANICS OF MATERIALS AND STRUCTURES

[msp.org/jomms](http://msp.org/jomms)

Founded by Charles R. Steele and Marie-Louise Steele

## EDITORIAL BOARD

ADAIR R. AGUIAR	University of São Paulo at São Carlos, Brazil
KATIA BERTOLDI	Harvard University, USA
DAVIDE BIGONI	University of Trento, Italy
MAENGHYO CHO	Seoul National University, Korea
HUILING DUAN	Beijing University
YIBIN FU	Keele University, UK
IWONA JASIUK	University of Illinois at Urbana-Champaign, USA
DENNIS KOCHMANN	ETH Zurich
MITSUTOSHI KURODA	Yamagata University, Japan
CHEE W. LIM	City University of Hong Kong
ZISHUN LIU	Xi'an Jiaotong University, China
THOMAS J. PENCE	Michigan State University, USA
GIANNI ROYER-CARFAGNI	Università degli studi di Parma, Italy
DAVID STEIGMANN	University of California at Berkeley, USA
PAUL STEINMANN	Friedrich-Alexander-Universität Erlangen-Nürnberg, Germany
KENJIRO TERADA	Tohoku University, Japan

## ADVISORY BOARD

J. P. CARTER	University of Sydney, Australia
D. H. HODGES	Georgia Institute of Technology, USA
J. HUTCHINSON	Harvard University, USA
D. PAMPLONA	Universidade Católica do Rio de Janeiro, Brazil
M. B. RUBIN	Technion, Haifa, Israel

**PRODUCTION** [production@msp.org](mailto:production@msp.org)

SILVIO LEVY Scientific Editor

---

See [msp.org/jomms](http://msp.org/jomms) for submission guidelines.

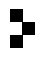
---

JoMMS (ISSN 1559-3959) at Mathematical Sciences Publishers, 798 Evans Hall #6840, c/o University of California, Berkeley, CA 94720-3840, is published in 10 issues a year. The subscription price for 2019 is US \$635/year for the electronic version, and \$795/year (+\$60, if shipping outside the US) for print and electronic. Subscriptions, requests for back issues, and changes of address should be sent to MSP.

---

JoMMS peer-review and production is managed by EditFLOW® from Mathematical Sciences Publishers.

PUBLISHED BY

 **mathematical sciences publishers**  
nonprofit scientific publishing

<http://msp.org/>

© 2019 Mathematical Sciences Publishers

# Journal of Mechanics of Materials and Structures

Volume 14, No. 3

May 2019

- 
- Experimental and numerical energy absorption study of aluminum honeycomb structure filled with graded and nongraded polyurethane foam under in-plane and out-of-plane loading**  
ALIREZA MOLAIEE and SEYED ALI GALEHDARI 309
- Transient thermal stresses in a laminated spherical shell of thermoelectric materials**  
YUE LIU, KAIFA WANG and BAOLIN WANG 323
- Tuning the propagation characteristics of the trapped and released strongly nonlinear solitary waves in 1-D composite granular chain of spheres**  
BIN WU, HEYING WANG, XIUCHENG LIU, MINGZHI LI, ZONGFA LIU and CUNFU HE 343
- Accurate buckling analysis of piezoelectric functionally graded nanotube-reinforced cylindrical shells under combined electro-thermo-mechanical loads**  
SHENGBO ZHU, YIWEN NI, JIABIN SUN, ZHENZHEN TONG, ZHENHUAN ZHOU and XINSHENG XU 361
- Thermoelastic fracture initiation: the role of relaxation and convection**  
LOUIS M. BROCK 393
- Development of fracture mechanics model of beam retrofitted with CFRP plate subjected to cyclic loading**  
SHAHRIAR SHAHBAZPANAH and HUNAR FARID HAMA ALI 413
- Assessment of degradation of railroad rails: finite element analysis of insulated joints and unsupported sleepers**  
HOSSAM ELSAYED, MOHAMED LOTFY, HAYTHAM ZOHN and HANY SOBH 429



1559-3959(2019)14:3;1-V